PCCP

Oscillator phase and the reaction dynamics of HN_3: A model for correlated motion

Karin R. Wright and John S. Hutchinson*

Department of Chemistry and Rice Quantum Institute—MS 60 Rice University, 6100 Main Street, Houston, TX 77005-1892, USA

Received 20th October 1998, Accepted 8th January 1999

The reaction coordinate for a unimolecular dissociation reaction is intrinsically anharmonic, therefore the period of vibration depends upon the energy in the bond. Consequently, the final few vibrations leading up to and including reaction can occur over very different time scales, depending upon the amount of vibrational energy in the reaction coordinate. In recent studies, we have compared ensembles of reactive trajectories and have observed correlations in molecular motions during reaction leading up to the transition state. If the comparison is made in time, differences in the periods of the reaction coordinate vibration can obscure these correlations. However, if the reactions are compared vibration by vibration (*i.e.*, coherently) clear patterns of vibrational motions emerge in the reaction dynamics. In this paper, we introduce a new application of the Hilbert transform to assign oscillator phases to the motions of anharmonic oscillators, which permits coherent comparison of trajectories. We also demonstrate by several examples that, when compared coherently, reaction dynamics of HN_3 exhibit order which is not evident in time series comparisons. These orderly patterns of motions reflect the intramolecular conditions necessary for reaction to occur. We propose a model to account for the observed correlated motion in terms of the requirements for intramolecular energy transfer. As a consequence of the constraints of energy transfer, the phases of several oscillators have clearly defined relative values. Physically this corresponds to a correlation in the vibrations of several modes such that (for example) two key bonds always extend simultaneously during the course of reaction. Since the motions of atoms preceding reaction are not random, but rather follow a specific pattern, a restricted set of reactant states immediately precede reaction.

1 Introduction

The fundamental processes of chemical reactions involve formation and breakage of bonds. Consequently, chemists have long pursued a detailed energetic and dynamic description of these processes. Molecules with sufficient energy to react may do so promply or may "predissociate", surviving for many cycles of vibration, even when the total energy is the same. The rate of unimolecular reaction is largely governed by the vibrational predissociation lifetime. What accounts for these differences in lifetimes? How does sufficient energy reach the reaction coordinate, permitting the bond to break? Is the reaction coordinate simply the bond that ultimately ruptures, or is it a more complex admixture of molecular motions? These are amongst the many questions addressed by the study of reaction dynamics.

Over the past decade, we have analyzed the classical dynamics of a variety of unimolecular reactions with the goal of understanding the vibrational dynamics and vibrational energy transfers that lead to the transition state of the reaction.[1–5] In each case, we have observed significant patterns of vibration in the final moments prior to reaction, indicating the existence of a highly specific path leading to the transition state. One or more vibrational modes, in addition to the bond or mode undergoing reaction, oscillate with a specific phase relationship with respect to the reaction coordinate. These phase correlations, which are observed when the reactive trajectories are referenced in time to the point of reaction, occur over several vibrational periods and, most significantly, result in a large scale, irreversible transfer of energy into the reaction coordinate immediately prior to reaction. We have referred to the latter phenomenon as "impulsive" energy transfer.

More recently, we have studied unimolecular reactive dynamics by sampling states at the transition state and propogating these backwards in time to sample the dynamics leading to the transition state. This type of analysis produces the same correlated vibrations prior to reaction, but also reveals that these correlations result from a highly structured vibrational phase space in the vicinity of the transition state. Our studies follow those of De Leon and co-workers[6–9] who first reported observation of "cylindrical manifolds" in the vibrational phase space of unimolecular reactions. In essence, they demonstrated that, in each unimolecular reaction, a "reactive cylinder" extends out from the transition state, and each reactive trajectory falls inside this cylinder. Hence, the reactive cylinder defines the specific path leading to the transition state.

In our previous paper,[4] we demonstrated that the location of the reactive cylinder in phase space could be predicted by energetic constraints placed on reactive trajectories during the final half-period of oscillation of the reaction coordinate. In this paper, we present further development in the energetic and dynamic description of molecular bond breaking, focusing on the details and origins of the specific phase correlations between reactive and non-reactive modes during the final few vibrations prior to reaction. We examine in detail the unimolecular dissociation of hydrozoic acid (hereafter referred to as HN_3), which reacts by rupture of the central N—N bond:

$$HN_3 \rightarrow HN + N_2$$

In our previous studies of unimolecular reaction, we have searched for patterns of motions during reaction by compar-

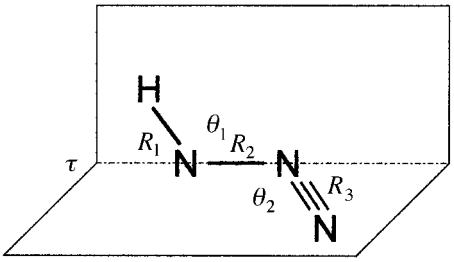

Fig. 1 HN_3 local modes.

ing large numbers of reactive trajectories using time as the independent parameter. Specifically, we choose a convenient point at or near the transition state along the reaction coordinate and define $t = 0$ at the crossing of that point. We then average local mode coordinates over the reactive ensemble at each instant prior to $t = 0$. Given that trajectories are generated as time series by integration of the equations of motion, and that time is the standard means of ordering events, this is a very reasonable approach, and has been useful in clearly revealing some of the details of correlated motion. However, in Section 3.1 we will show that, because of anharmonicity, time comparisons have intrinsic limitations which affect the analysis of reactive dynamics.

In Section 3.2 we show that many of these limitations associated with anharmonicity are circumvented by comparing reaction dynamics vibrational phase by vibrational phase (*i.e.*, coherently), irrespective of the time periods associated those motions. We also introduce a new application of the Hilbert transform, which makes coherent study of reaction dynamics feasible even when the Hamiltonian involves coupled anharmonic oscillators.

In Section 5 we introduce a model for correlated motion which addresses the preceding questions. This model makes a number of predictions regarding the expected characteristics of correlated motion, and these are verified in Section 5.1. Lastly in Section 6 we discuss our conclusions and their implications.

2 The HN_3 Hamiltonian

Hydrazoic acid (HN_3) can dissociate into diatomic fragments HN and N_2 by undergoing a singlet to triplet electronic transition.[10,11] The transition can be viewed as the result of an electronic surface crossing between the ground state of the HN_3 parent molecule with an excited state which correlates to the ground $^1\Sigma_g$ state of the N_2 product and the ground $^3\Sigma$ state of the HN product. The crossing occurs when the central N—N bond of the parent is extended to a length of 3.5 a_0, an event which requires an energy of 12 700 cm^{-1} (1.52 eV or 147 kJ mol^{-1}). In this study we are primarily concerned with the vibrational events which produce the activation of the N—N reaction coordinate and not with the electronic events which determine whether curve crossing occurs. Hence we have focused on the events on the ground electronic surface of the parent molecule which lead to an extension of the N—N bond to 3.5 a_0. We therefore use the potential constructed by Julien *et al.*[2], which is defined in terms of internal coordinates R_1, R_2, R_3, θ_1, θ_2, and τ, as shown in Fig. 1.

2 Oscillator phase analysis *via* the Hilbert transform

3.1 Phase complications arising from anharmonicity

Any vibration capable of unbound motion, including the reaction coordinate, must be fundamentally anharmonic. Anharmonic oscillators have the property that (unlike their

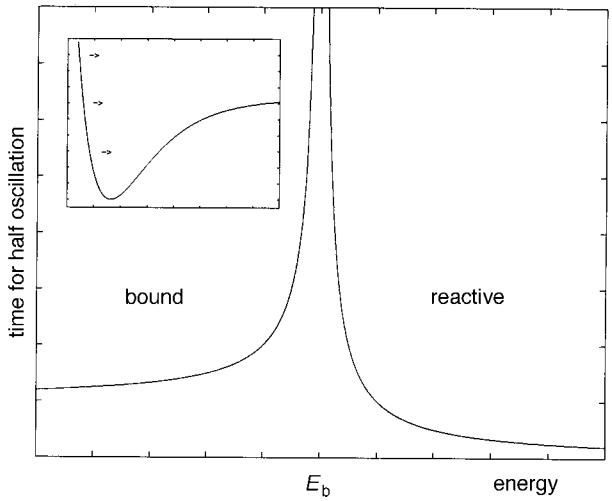

Fig. 2 Schematic illustration of the transit time for half oscillation, from the last inner turning point to either the transition state or the outer turning point, depending upon the energy in the reaction coordinate, *vs.* energy in the reaction coordinate. The pole corresponds to a reaction coordinate energy equal to that of the barrier. The inset figure shows a prototypical example of an anharmonic potential, with the arrows indicating reactive, asymptotic and bound energies from top to bottom, respectively.

harmonic counterparts) the period of oscillation depends upon the oscillator energy, so very similar processes can occur over very different time scales. Consider the time necessary for a bond to go from maximum compression to maximum extension (one-half of a vibrational period) when the bond is anharmonic; as illustrated by a Morse oscillator in the inset of Fig. 2. As Fig. 2 illustrates, at low energies for such an oscillator this time is related to the harmonic frequency since near equilibrium the differences between harmonic and harmonic and anharmonic potentials are small. As we increase the energy in the bond, the time for extension increases; as the energy in the bond approaches the dissociation energy (E_b) the time to maximum extension approaches infinity. As we further increase the energy in the vibration the bond breaks thereby allowing unbound motion and under these conditions we define the maximum extension of the bond to be the transition state. As energy in the bond increases above E_b the time to extend beyond the transition state decreases as the fragments separate with increasing velocity. The behavior of bond extension time as a function of energy is illustrated in Fig. 2. The implication of this time response is that, for anharmonic oscillators very similar motions can occur over very different time scales, searching for similarities in these motions by means of time comparisons can be misleading.

Fig. 2 represents a generic anharmonic oscillator, so it is reasonable to determine whether the complications suggested by Fig. 2 are actually manifest when comparing trajectories. Fig. 3 demonstrates that such problems do arise when looking for patterns of atomic motions by taking time averages of local mode values. In this figure we plot bond length of the

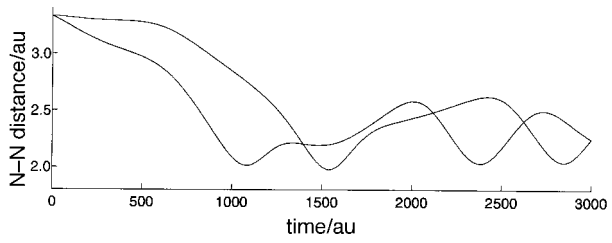

Fig. 3 Bond length for the reaction coordinate as a function of time for two trajectories with the same total energy, 1.05E_b.

reaction coordinate as a function of time for two trajectories with the same total energy, but which differ slightly in the energy in the reaction coordinate. We focus on the final moments of reaction by defining the zero of time to be when the molecules are at the transition state and positive time to correspond to the reactant state of the molecules. Note that, although these two trajectories begin at the same instant with the same maximum extension in the reaction coordinate, within roughly one vibration (at $T \approx 2400\ E_h$), the bond is at maximum compression in one trajectory, while in the other one the same bond length is at nearly maximum extension. A time average of the motions of this vibration for these two trajectories will result at $T \approx 2400\ E_h$ in an average bond length value, which is roughly the equilibrium value. This does not properly reflect the behavior of either trajectory, and therefore contains little information about patterns of motions during reactions.

The types of problems illustrated in Fig. 3 arise because in the anharmonic case periods of vibrations differ. One approach to circumvent these problems is to compare reactive trajectories not in time but rather phase by phase, *i.e.*, coherently. Comparing trajectories coherently is not a new idea, but in the next section we introduce a new application of the Hilbert transform that makes coherent comparison feasible for systems with coupled anharmonic oscillators, thereby making coherent comparison more readily applicable to chemically interesting systems.

3.2 Anharmonic oscillator phase and the Hilbert transform

The advantages of comparing trajectories in phase have been noted previously.[12] The standard means of tranforming from time to oscillator phase is by the action–angle transform,[13] which involves integration over a closed path and so applies only to trajectories with periodic orbits. In practice this is accomplished by decoupling the vibrations of interest and approximating each mode as an independent oscillator (either harmonic or anharmonic). The required approximations for this form of phase analysis are frequently large, particularly when significant couplings must be neglected.

Fig. 4 shows momentum as a function of time (solid line) for a single cycle of vibration of an anharmonic oscillator (modelled in this instance by a Morse function with $E_b = 0.1\ E_h$ and $\alpha = 1$, where α is the coefficient in the exponential argument in the Morse potential function). The relative energy of vibration is $(E/E_b) = 0.9$ resulting in motion that is clearly significantly anharmonic. However, when we assign phase values to this anharmonic motion using the action–angle transform, the resulting phases (shown by the dot-dashed line) are linear in time, consequently comparisons made using action–angle phase will suffer many of the same liabilities as a direct time comparison. By contrast, the phase assigned to this anharmonic motion by the Hilbert transform (dashed line), as defined below, is distributed uniformly within a cycle of oscillation rather than uniformly in time. This may be verified by noting that for the first quarter cycle of vibration (*i.e.*, from $p = 0$ to $p = p_{max}$) the Hilbert transform assigns $(\pi/2)$ phase values and similarly for the next quarter cycle ($p = p_{max}$ to $p = 0$). The Hilbert transform phase therefore has the desirable property that (unlike the action–angle phase) each phase value can be uniquely associated with a specific stage of the cycle of vibration, irrespective of the energy or the degree of anharmonicity of the vibration. Thus the Hilbert transform oscillator phase is appropriate for use with coherent comparison of trajectories.

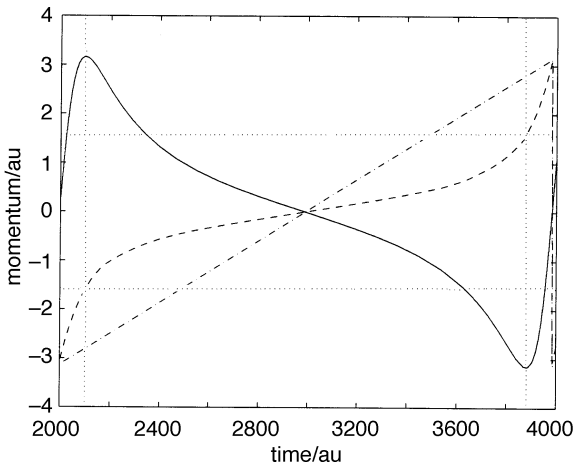

Fig. 4 A single cycle of oscillation for a Morse oscillator with $(E/E_b) = 0.90$. (—) scaled momentum; (—·—·) action–angle transform phase; (– – – –) Hilbert phase. The dotted lines demonstrate that at equilibrium (*i.e.*, the extrema of momentum) the Hilbert phase is $\pm(\pi/2)$, while the corresponding action–angle phase is nearly $\pm\pi$.

The Hilbert transform is a well known technique that finds applications in fields as diverse as engineering,[14] optics,[15] and geophysics.[16] Within chemistry, it has been applied to a variety of problems, primarily in the area of spectroscopy.[17,18] Absorption and dispersion spectra are Hilbert transforms of each other,[19] and may be combined to diagnose line broadening mechanisms in NMR[20] and EPR spectra.[21]

The Hilbert transform may be adapted to assign oscillator phases to atomic motions as follows. The transforms itself[22] is the principal part of the following integral:

$$F(t) = \frac{1}{\pi} \int_{-\infty}^{+\infty} \frac{f(t')\,dt'}{t' - t} \tag{1}$$

where $f(t)$ is the time series comprising one mode of vibration, and is readily obtained as a component of a trajectory. Note that eqn. (1) is equivalent to convolving the $f(t)$ time series with $(-1/\pi t)$, which leads to an efficient numerical implementation of the transform.[22] The convolution of $f(t)$ by $(-1/\pi t)$ is replaced by equivalent operations in the Fourier transform domain, thus we Fourier transform $f(t)$ to $F(s)$ and $(-1/\pi t)$ to isgn(s). Inverse Fourier transformation of the product isgn(s)$F(s)$ yields the equivalent of the time domain convolution.

Having obtained $F(t)$ (the Hilbert transform of a mode's vibration as a function of time) either numerically or by direct evaluation of eqn. (1), one next forms what Bracewell terms the quadrature function[22]

$$Q(t) = f(t) + iF(t) \tag{2}$$

a function in complex cartesian coordinates which may in turn be transformed into complex polar coordinates ($re^{i\phi}$) by the following relationships:[23]

$$r(t) = (f(t)^2 + F(t)^2)^{1/2} \tag{3}$$

$$\phi(t) = \tan^{-1}\left(\frac{f(t)}{F(t)}\right) \tag{4}$$

where $r(t)$ is oscillator amplitude as a function of time, and $\phi(t)$ is the oscillator phase corresponding to the vibration of the $f(t)$ local mode.

One advantage of the Hilbert transform is that it can be directly applied to local mode motions so the transform is not affected by details of the Hamiltonian which generated the local mode vibrations. Thus the Hilbert transform (unlike the action–angle one) is applicable to systems with coupled anharmonic oscillators, and is not restricted to evaluation of periodic orbits. The Hilbert transform is therefore a tool of great generality and utility for assigning oscillator phase values to the motions of arbitrary molecular vibrations. In the next section we will show that when studied in terms of oscillator phase interesting patterns of motions emerge in the reaction dynamics of HN_3.

4 Phase and reaction dynamics

Our objective in comparing reactive trajectories is to identify similarities or correlations in the reaction dynamics. When essentially all trajectories execute a similar sequence of motions during reaction, those motions contain information about conditions necessary within the molecule for reaction to occur. In this section we present a number of examples which show that, when studied in phase, the reaction dynamics of HN_3 are not random but, because of anharmonicity, may appear to be random when studied in time.

The upper plot in Fig. 5 shows momentum for the terminal N=N stretch during reaction (which cleaves the central N—N bond) as a function of time for fifty reactive trajectories, where zero time is defined to be the transition state and positive times correspond to the molecule as a reactant. If we were to look for patterns of motions by averaging momentum values for all trajectories as a function of time the result would be an average momentum that hovers near zero. By contrast, consider the lower plot in Fig. 5, which shows momentum for the N=N local mode for the same fifty trajectories displayed now with the independent axis as phase of the reaction coordinate (a different local mode). This figure shows that when parameterized by oscillator phase, for a portion of the reactive process (*i.e.*, from $\phi \approx 2$ to $\phi \approx 2\pi$) the reaction dynamics of this local mode shows a clear pattern, such that nearly all trajectories have first negative then sharply positive momenta. This result is surprising in two respects: first, all these reactive trajectories (whose initial conditions were selected randomly) follow the same pattern of motion; and second, the pattern of motion is evident when we study the motions of this local mode of vibration as a function of the phase of the vibration of a different local mode. The physical interpretation of this result is that, for a portion of the reaction process, the motions of the reaction coordinate (the central N—N bond) and the terminal N=N stretch are not independent: a fixed relationship exists between the phases of the two vibrations, which we term "correlated motion".

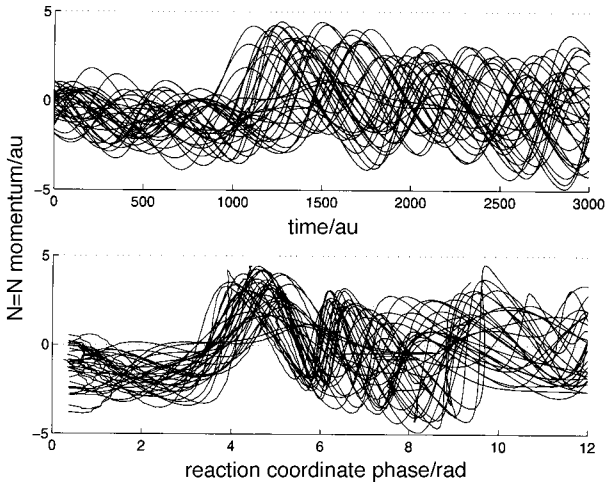

Fig. 5 Vibration of the N=N local mode for fifty reactive trajectories with the same total energy. $1.05E_b$, where zero time corresponds to the transition state and increasing times to reactant states of the molecule. In the upper figure the motions are presented as a function of time, while in the lower figure the same motions are presented as a function of the phase of the reaction coordinate (the central N—N bond).

Fig. 6 shows a more systematic means of identifying phase relationships between local modes and the reaction coordinate during reaction (*i.e.*, correlated motion). The *y*-axis in each of these figures is the phase (modulus 2π) of a given local mode, and the *x*-axis is the continuous phase of the reaction coordinate, such that $\phi = 0$ corresponds to the transition state, $\phi = 2\pi$ to the outer turning point of the final cycle of vibration of the reaction coordinate, and $\phi = 4\pi$ to the outer turning point of the penultimate vibration of the reaction coordinate. For roughly one hundred reactive trajectories we assign phase values to the vibrations of all local modes using the Hilbert transform, and then (in separate plots) the instantaneous pairings of phase values for each local mode and the reaction coordinate are assigned to a bin, based on their particular values. For any given local mode, when all phase values for every reactive trajectory are distributed, the binned phase values are then represented by a contour plot, where the contours delineate bins with two, three or four times the average number of points. The resultant plots in Fig. 6 show that, when no correlation exists between the motions of a given local mode and the reaction coordinate (such as in the case of the H—N stretch local mode), the phase pairings are

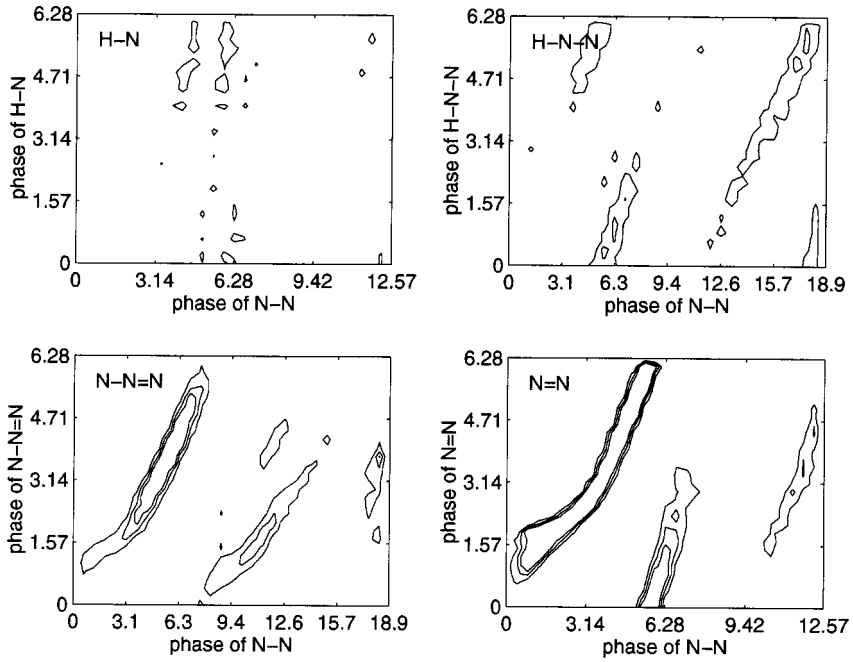

Fig. 6 Contoured phase maps of the local modes for 100 HN_3 trajectories with $1.1E_b$ total energy. Phases are in radians. Note that the local mode phase is modulus 2π while that of the reaction coordinate is continuous. The contours, respectively, enclose areas with 2, 3 and 4 times the average population, thus identifying favored phase relationships.

random and so are distributed roughly uniformly. By contrast, the contoured phase map for the terminal N=N stretch shows that the motions of this local mode are strongly correlated with those of the reaction coordinate. Knowledge of the phase of the reaction coordinate allows one to predict with great confidence a relatively narrow range of phase values for the N=N local mode (since the contours identify a well defined region in which most phase pairings occur).

The contoured phase maps therefore show that just before reaction, for nearly a full cycle of vibration of the reaction coordinate the motions of the central N—N bond and the terminal N—N bond synchronize and that in the final vibration of every reaction both bonds contract simultaneously. When the phase of the reaction coordinate exceeds $\approx 2\pi$ (*i.e.*, in vibrations preceding the final period), the motions of these two bonds no longer correlate. The extent of correlated motion is indicated by the narrowness and height (*i.e.*, number of contours) of the regions of favored phase relationships, thus the N=N local mode shows strongly correlated motion, the two bending modes H—N—N and N—N=N show correlated motion to a lesser degree, and the H—N local mode lacks any degree of correlated motion.

In a final example of organization in reaction dynamics evident in phase, we begin by looking at the logarithmic decay curves for several normal mode excitations of HN_3, shown in Fig. 7. These decay curves were generated by randomly assigning initial conditions (within the constraints of the normal mode energy distribution specified for each state) for five hundred trajectories and then noting the time at which reaction occurs. We will focus on those choices of initial conditions that result in rapid reaction, therefore the decay curves are limited to a maximum time of 0.1 ps. The normal modes selected correspond to a single energy of 3.2 E_b, where excess energy has been distributed between the terminal N=N stretch and the terminal N—N stretch. (In these calculations each normal mode was assigned to least zero point energy.) Recall that Fig. 6 demonstrated that the H—N stretch has no correlated motion, while that of the N=N stretch is strongly correlated. What is the effect of distributing excess energy into these very different modes?

We adopt a notation to describe an initial energy distribution by using a set of six quasi-classical quantum numbers (v_1, v_2, v_3, v_4, v_5, v_6), each describing the initial vibrational state of one of the six normal modes of HN_3. Thus, we will study the reaction dynamics for three cases: the (0 15 0 0 0 0) state where an excitation of $\approx 3E_b$ is placed into the N=N stretch, the (3 10 0 0 0 0) state where the H—N excitation is $\approx E_b$ and that of N=N is $\approx 2E_b$ and lastly the (6 6 0 0 0 0) state with an initial H—N excitation of $\approx 2E_b$ and N=N excitation of $\approx E_b$.

In Fig. 7, we examine the unimolecular reaction kinetics by plotting log A/A_0, where A is the number of unreacted trajectories of time t, and A_0 is the total number of trajectories in the ensemble. A number of observations can be made from the decay curves of Fig. 7. First, the reaction rates for HN_3 are state specific, with increased excitation in the N=N stretch (which has correlated motion) resulting in faster rates of reaction than the states that have large excitations in the H—N mode (which does not have correlated motion. Second, the state specific kinetics are not first order (as would be indicated by a decay curve corresponding to a single exponential), but rather are more complex, corresponding to multiple exponentials. We will focus upon the faster reactions (*i.e.*, those occuring within 0.045 ps), corresponding to the first roughly linear region of each decay curve. Even over this brief range the local rate constant (defined by the slope of the approximately linear segment) varies from state to state. Third, even within a single state, some initial conditions result in rapid reaction, while others result in relatively long lived molecules. Recall that within a single state both the total energy and the distribution of internal energy is the same for every trajectory, so the initial amplitudes of vibration for any given normal mode are equal in every trajectory. The essential difference between initial excitations is not oscillator amplitude (which defines energy), but rather is oscillator phase.

Since differences in initial conditions result in trajectories of greatly different lifetimes and those differences correspond to variations in initial normal mode phases, we seek to identify relationships between the initial phases and trajectory lifetimes. We do so in a very direct manner, by plotting initial phase of the N=N oscillator against initial phase of the N—N reaction coordinate and against the inverse of the lifetime of a trajectory. We selected to plot the initial phase of the N=N vibration both because it is the mode that receives a substantial initial excitation and because this mode has correlated motion. We selected as the orthogonal axis the phase of the N—N vibration because this motion defines reaction in HN_3. Inverse time to reaction was selected because this axis emphasizes our objective, *i.e.*, the conditions required for rapid reaction. The resulting plots are shown in Fig. 8–10, where (inverse) time to reaction for each rapidly reacting trajectory (*i.e.*, a lifetime of ≤ 0.045 ps) is plotted in three-dimensions against the initial phases. To emphasize the

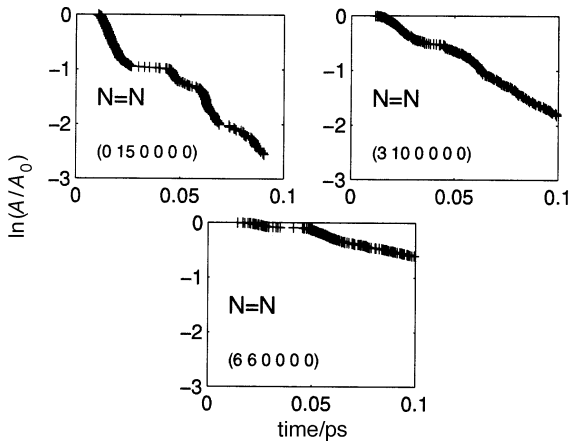

Fig. 7 Logarithmic decay curves for N=N, N—N and HNN normal mode excitations of HN_3, showing the fraction of unreacted trajectories, A/A_0, as a function of time. Each data set represents five hundred trajectories whose total energy is 3.2 E_b. Initial energy distributions are given by the set of six quantum numbers (v_1, v_2, v_3, v_4, v_5, v_6) in each figure. The axes are selected to emphasize rapid reactions.

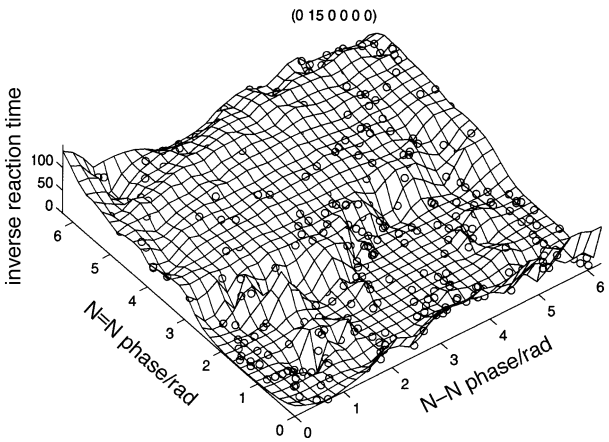

Fig. 8 Relationship for the initial energy distributions (0 15 0 0 0 0) between the inverse time to reaction (in inverse picoseconds) and the initial phases of the reactive N—N normal mode and the N=N normal mode. This plot includes only those trajectories reacting within 0.045 ps.

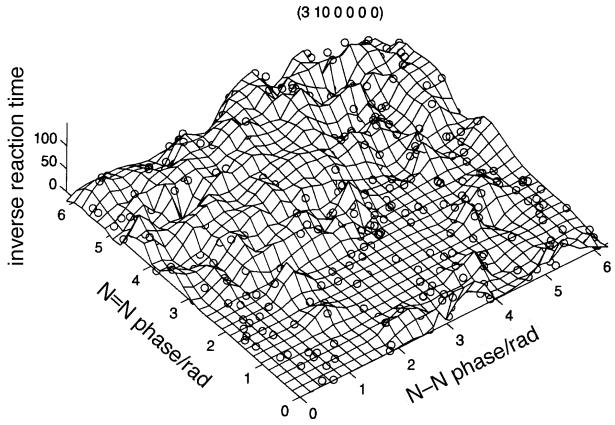

Fig. 9 Relationship for the initial energy distribution (3 10 0 0 0 0) between the inverse time to reaction (in inverse picoseconds) and the initial phases of the reactive N=N normal mode and the N=N normal mode. This plot includes only those trajectories reacting within 0.045 ps.

three-dimensional relationship between data points (for easier identification of trends within the distribution) a mesh grid is fitted to the distribution of lifetimes, so that rapid reactions are identified as peaks, and slower reactions as valleys.

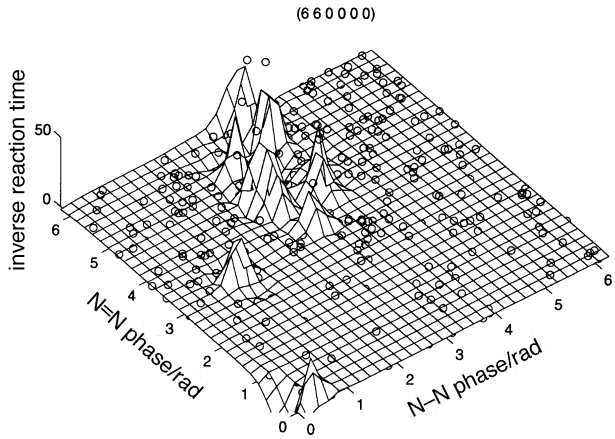

Fig. 10 Relationship for the initial energy distribution (6 6 0 0 0 0) between the inverse time to reaction (in inverse picoseconds) and the initial phases of the reactive N—N normal mode and the N=N normal code. This plot includes only those trajectories reacting within 0.045 ps.

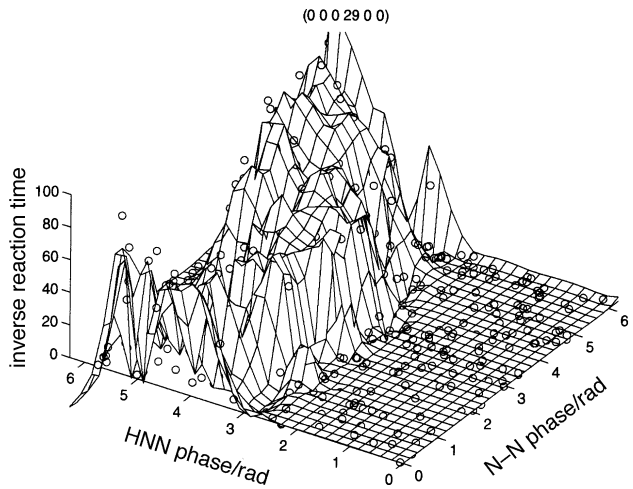

Fig. 11 Relationship for the initial energy distribution (0 0 0 29 0 0) between the inverse time to reaction (in inverse picoseconds) and the initial phases of the reactive N—N normal mode and the HNN normal mode. This plot includes only those trajectories reacting within 0.050 ps.

Fig. 8 shows the resulting relationship for the (0 15 0 0 0 0) state, in which the initial excitation is all within the N=N normal mode. Under these conditions, all trajectories where the initial N=N excitation is between π and 2π react rapidly, and the relatively few longer lived trajectories all have initial N=N phases between 0 and π. Fig. 9 shows the case for the (3 10 0 0 0) state, where the initial excitation in the N=N normal mode is $\approx 2E_b$. A smaller initial excitation in the N=N mode, which correlates to the reaction coordinate (with a corresponding increase in the initial H—N excitation, which does not), results in fewer swiftly reacting trajectories. However, when viewed in terms of the initial phase assignment both rapidly reacting and long lived trajectories are defined by distinct regions of initial phases. Finally, we consider the (6 6 0 0 0 0) state in which the initial excitation is distributed with $\approx E_b$ in the N=N normal mode with the balance of the available energy in the H—N normal mode. Relatively few trajectories react rapidly under these conditions, but Fig. 10 shows that those which do react swiftly nearly all conform to a very restricted set of initial phases. We conjecture that the phase relationships evident are a consequence of conditions necessary in HN_3 for energy transfer between modes, and in the next section we address this issue.

We have chosen examples of order evident in phase for the reaction dynamics of HN_3 that emphasize the clearest case, *i.e.*, the interactions between the terminal N=N stretch and the reaction coordinate. However, other modes also show similar patterns of order, as is demonstrated in Fig. 11 where the initial excitation of $\approx 3E_b$ is placed in the H—N—N bending mode. In this case, rapidly reacting trajectories also have a clear domain of initial phase values.

5 A model for correlated motion

In the previous section we showed several examples where in every reactive trajectory the motions of several local modes of HN_3 are synchronized during the final two vibrations that precede reaction. We now propose a model to account for the existence of this correlated motion.

Consider a system with barely sufficient energy to react. There is only a single trajectory that can transit the lowest potential energy position of the transition state with essentially zero momentum. What are the necessary characteristics of this lowest energy reactive trajectory? In all vibrations preceding the final one, the reaction coordinate has less energy than that required for reaction. Since the system contains barely sufficient energy to permit reaction, this lowest energy reactive trajectory must be the most efficient one in gathering all possible energy from other modes. The motions preceding reaction of the lowest energy trajectory are those that permit maximum energy transfer from all other modes into the reaction coordinate. Since energy can only move between modes when they couple, the path of the lowest energy trajectory must coincide with regions of phase space where modes are strongly coupled. The lowest energy reactive trajectory must therefore represent a very specific path, *i.e.*, the one that permits maximum energy transfer so that sufficient energy accrues in the reaction coordinate to permit crossing the transition state.

Let us now slightly increase the energy available to the system, so that the energy required for reaction is a somewhat smaller proportion of the total energy. This corresponds to sampling a small region at the transition state, rather than a single point. These nearly lowest energy trajectories are also constrained to visit regions of phase space with high couplings to gather sufficient energy to react. Whether or not a system demonstrates correlated motion (*i.e.*, a restricted set of vibrational phase values) depends upon the nature of the Hamiltonian. If the Hamiltonian is such that one or more orthogonal modes couple strongly to the reaction coordinate, and the

regions of strong coupling are compact (*i.e.*, correspond to a limited range of phase values), then the system will demonstrate correlated motion, because all the nearly lowest energy trajectories will traverse substantially the same region of phase space as the lowest energy trajectory. However, if the Hamiltonian is such that no mode couples strongly to the reaction coordinate and such coupling regions as do exist are small and scattered, then the next to lowest energy trajectories may easily diverge from the vicinity of the lowest energy trajectory, and no correlated motion will be observed.

In light of the preceding arguments regarding the behavior of low energy reactive trajectories, we propose a model for correlated motion as follows:

Correlated motion is a consequence of energy transfer from orthogonal modes into the reaction coordinate *via* high coupling regions in the Hamiltonian isoergic surface. Correlated motion results when these high coupling regions of the Hamiltonian correspond to a limited range of oscillator phase values.

This model for correlated motion makes a number of verifiable predictions, including: 1. Coupling during the final stages of reaction should be greater than in preceding vibrations. 2. Modes that are strongly coupled to the reaction coordinate exhibit correlated motion. Conversely, modes without correlated motion should not couple to the reaction coordinate. 3. In systems with correlated motion, the strength of that correlation should decrease with increasing energy in the system.

To test the validity of the proposed model for correlated motion in the following sections each of the preceding predictions is examined.

5.1 The first prediction: strong coupling

To test the first prediction we need a measure of coupling. One such simple measure is to define coupling energy, E_c, as the absolute energy difference between the full Hamiltonian H and the Hamiltonian H_0, in which all coupling terms have been set to zero:

$$E_c = |H - H_0| \tag{5}$$

A fundamental test of this model for correlated motion is to compare values of the coupling energy during the final vibration to those in preceding ones. Fig. 12 shows E_c *vs.* phase of the reaction coordinate for one hundred HN_3 trajectories when the available energy is $1.05E_b$, where E_b is the bond energy of the N—N dissociation. As will be shown shortly,

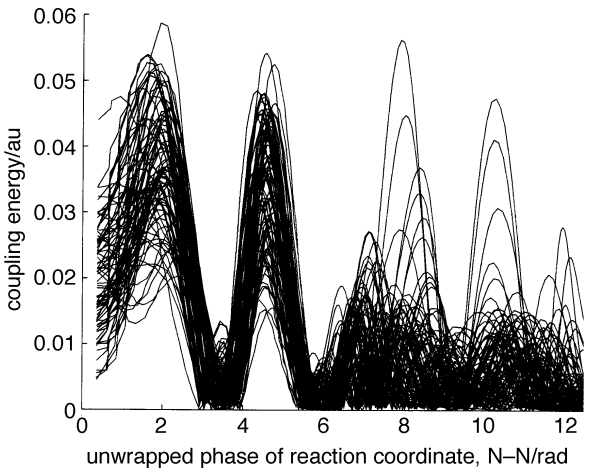

Fig. 12 Coupling energies for 100 HN_3 trajectories with $1.05E_b$ as a function of continuous reaction coordinate phase, where $\phi = 0$ corresponds to the transition state, and $\phi = 2\pi$ to the outer turning point of the final vibration preceding reaction of the reaction coordinate.

these trajectories exhibit strongly correlated motion. There is clearly on average a much higher level of coupling energy in the final vibration ($\phi = 0$, 2π) than in the preceding one, in accordance with the prediction.

However, Fig. 12 reveals other interesting trends. In the next to last cycle ($\phi = 2\pi$, 4π) the coupling energy for almost all trajectories is much less than that of the final cycle and occurs at random stages within the vibration. In stark contrast, during the last vibration prior to reaction ($\phi = 0$, 2π) the coupling is both large and systematic. For phases in the range from $(\pi/2)$ to 2π there is a clear pattern. E_c is nearly zero at $\phi = \pi$ and 2π (corresponding to turning points of the vibration) and reaches peak values at $(\pi/2)$ and $(3\pi/2)$ (where the vibration is passing through equilibrium). Relating these phase values to vibrational motion of the atoms reveals that during the last cycle coupling energy is least at the inner and outer turning points of the vibration, and is greatest near equilibrium. Thus coupling is least when the atoms' momenta are zero and is greatest when the momenta are maximum, suggesting that kinetic coupling plays a significant role in the system, even though the potential energy function for this Hamiltonian includes sizable potential coupling terms.[2]

Little emphasis should be placed upon the observations in the phase range of $\phi = 0$–$(\pi/2)$, since close to the transition state phase assignment becomes problematic. The inability of the Hilbert transform to assign phases to motions all the way to the transition state is not an algorithmic limitation, but rather is a consequence of the nature of the motion. Phase is only meaningful in the context of cyclic motion, and the process of reaction is intrinsically non-cyclic. As the reaction coordinate approaches the transition state, at some point the bond extends beyond the limits of previous cycles of vibrations. From this point onwards the motion is no longer cyclic so phase assignment becomes meaningless. Fortunately this "black-out zone" is small, involving at worst less than a quarter cycle of the final vibration. Still, because of this phenomenon it is difficult to ascertain if the loss of organization in E_c in the range from 0 to $(\pi/2)$ is real or is an artifact of the transformation to phase.

5.2 The second prediction: strong coupling and correlated motion

We have developed a simple and visual diagnostic for correlated motion which we will use to verify the second prediction, namely that correlated motion exists if and only if the local mode in question couples to the reaction coordinate.

We are seeking to identify patterns in the motions of atoms during reaction, but time comparisons have limitations because of anharmonicity, and phase is undefined in the immediate vicinity of the transition state. We therefore define a "reaction progress" coordinate, which is a line integral around the phase space ellipse of the reaction coordinate, as follows:

$$A = \int_1 \mathrm{d}s \tag{6}$$

$$\mathrm{d}s = \sqrt{\mathrm{d}p'^2 + \mathrm{d}q'^2} \tag{7}$$

where A is the reaction coordinate arc length and $\mathrm{d}p'$ and $\mathrm{d}q'$ are, respectively, the incremental momenta and coordinates for this oscillator, scaled in a manner that eliminates the effects of the fundamental differences in their units.[2] The sole objective for this rather elaborate measure of pseudo-time is to have a measure of reaction progress that is defined all the way to the transition state but is less susceptible to the complicating effects of anharmonicity than is time.

To identify correlated motion in a given local mode we plot the space curves corresponding to local mode position and momenta expressed as a function of reaction coordinate arc length, our measure of reaction progress. (Reaction progress of zero corresponds to the transition state while positive

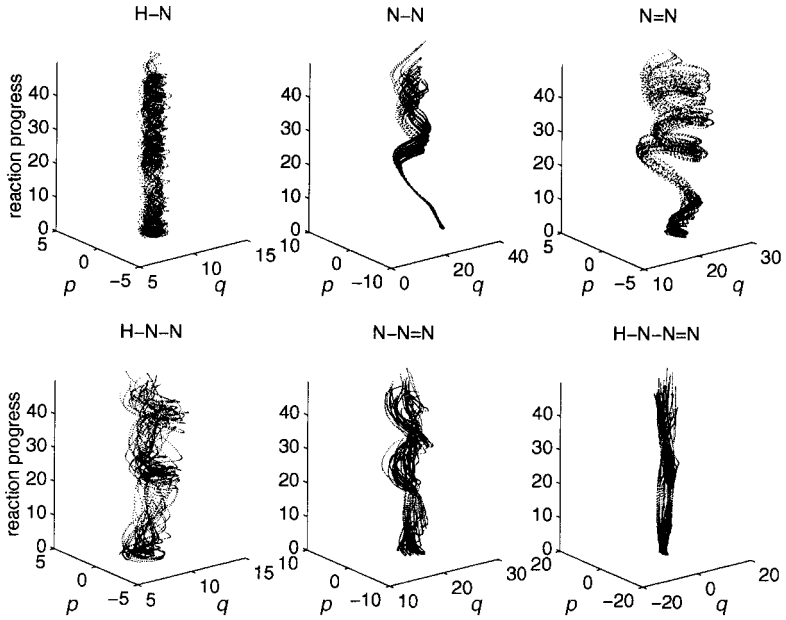

Fig. 13 Tornado plots of HN_3 local modes when the total energy is $1.1E_b$. q and p are coordinate and momentum in atomic units in the local mode labelled in each plot.

values correspond to the molecule as a reactant.) Over a single cycle of vibration the position and momentum values will trace out an ellipse, and when one includes a pseudo-time z-axis the resulting space curve is roughly helical, where the radius of the gyration is related to the energy of vibration. If for a single local mode one plots the space curves arising from many trajectories, a local mode will exhibit one of two classes of behaviour. In the absence of correlated motion the space curves form a featureless cylinder, but when correlated motion exists the trajectory paths cluster together in phase, spanning only a fraction of the energetically allowed values.[4] Fig. 13 shows an example of this diagnostic, which for obvious reasons we have named a tornado plot.

We have hypothesized that correlated motion arises as a consequence of couplings between the reaction coordinate and orthogonal modes. An advantage of computer simulations is that we are able to test the hypothesis directly by identifying the critical terms in the molecular Hamiltonian. For this purpose we selected the N=N local mode, because its correlated motion is clearest. If the correlated motion of the terminal N=N stretch is a consequence of coupling between that mode and the reaction coordinate, we should be able to identify specific terms within the Hamiltonian responsible for that coupling and removal of those terms should eliminate the corresponding correlated motion. In Fig. 14 we see precisely that result. In the left tornado plot (generated by the full Hamiltonian) we see the swirling pattern characteristic of correlated motion. By contrast, the right tornado plot (generated by a Hamiltonian which sets to zero the two elements of the Wilson $\boldsymbol{G}$ matrix,[24] which kinetically couple the N=N local mode to the reaction coordinate) shows the featureless cylinder characteristic of absence of correlated motion. This result is surprising from two perspectives. The changes to the Hamiltonian that eliminated the correlated motion of N=N are small, involving only two of the thirty six elements of the $\boldsymbol{G}$ matrix, so tiny changes to the Hamiltonian can have major impact upon the reaction dynamics, but only if the changes involve the critical elements. In the HN_3 Hamiltonian the terminal N=N stretch couples to the reaction coordinate in both the kinetic and the potential terms. When one repeats this experiment but instead eliminates only the potential coupling term (leaving the kinetic coupling intact) the N=N local mode still has strongly correlated motion. Thus, in HN_3 the kinetic coupling term is solely responsible for the strong correlation between the terminal N=N stretch and the reaction coordinate. This is consistent with the observations in Fig. 12, which show maximum coupling energy coincident with maximum momentum of the reaction coordinate, suggesting that, for HN_3, kinetic couplings (which have greatest impact when the momentum is maximum) are the critical factor in energy transfer.

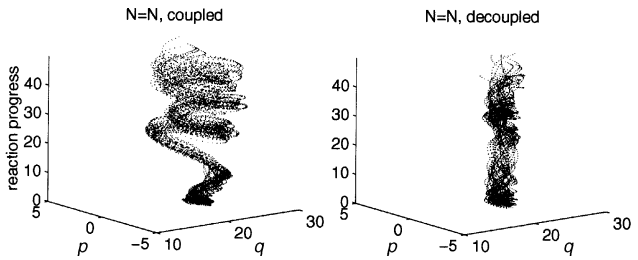

Fig. 14 Tornado plots of the N=N local mode, the left corresponding to a complete Hamiltonian and the right to one in which the $\boldsymbol{G}$ matrix term coupling p_{N-N} to $p_{N=N}$ is set to zero. (Total energy is $1.1E_b$.) q and p are coordinate and momentum in atomic units in the N=N local mode.

Tornado plots are an appealing visualization of reaction dynamics, but are somewhat qualitative. A more quantitative diagnostic for correlated motion is the contoured phase plot, which shows the extent to which favored phase pairings exist for a given local mode and the reaction coordinate. When the two modes are uncorrelated the relationship of their phases is random and the resulting contour plot is featureless, as is the case for the H=N stretch in Fig. 6. However, when the local mode correlates with the reaction coordinate the contoured phase map will identify the favored phase pairings that are a consequence of that correlation. (See the N—N=N=N plots in Fig. 6.) Thus contoured phase maps are a more quantitative diagnostic for correlated motion, but the outcome is fully consistent with the tornado plots and serve also to verify prediction 2, showing that those modes which couple to the reaction coordinate have correlated motion, while those modes which are isolated do not.

5.3 The third prediction: decreasing correlation with increasing energy

The final prediction of our model deals with changes in correlated motion as a function of increasing molecular energy. We interpret correlation to be a consequence of the molecular

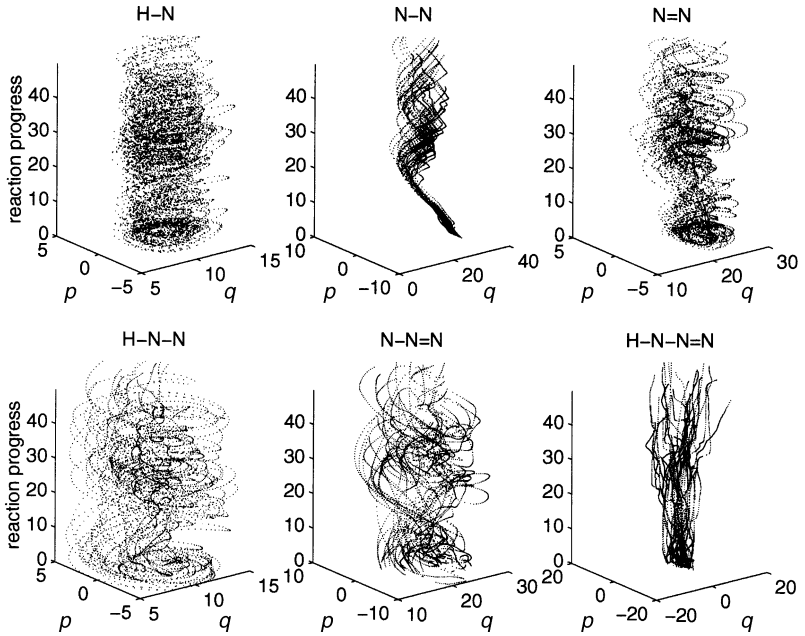

Fig. 15 Tornado plots of HN_3 local modes when the total energy is $3.2E_b$. q and p are coordinate and momentum in atomic units in the local mode labelled in each plot.

conditions required for energy transfer into the reaction coordinate. When the molecular energy is such that reaction requires most of the internal energy in the molecule to reside within the breaking bond, the conditions that permit this degree of energy transfer are narrowly constrained, resulting in highly correlated motion. However, (in a higher energy case) as the energy required to break the bond becomes a smaller fraction of the total available energy, a greater number of molecular configurations can satisfy the conditions for energy transfer and a smaller extent of correlated motion results. We therefore predict that correlated motion should decrease with increasing energy in the molecule.

Fig.15 shows tornado plots for HN_3 when the total internal energy is $3.2E_b$. When this figure is compared to Fig. 13 where the comparable internal energy is $1.1E_b$ it is evident (particularly in the case of the terminal N=N stretch) that the organization characteristic of correlated motion is much less the higher energy case. However, the tornado plot remains a rather qualitative diagnostic tool for correlated motion and for this prediction a more quantitative measure is required. We use contoured phase plots to quantitatively assess the change in correlated motion with energy and again (because of its clarity) select the terminal N=N stretching mode to characterize correlated motion. In Fig. 16 we show contoured phase plots for the terminal N=N stretch for energies ranging from $1.1E_b$ to $3.2E_b$. The plots show a clear trend where increasing energy corresponds to diminished organization of the favored phase pairings (*i.e.*, correlated motion). When the

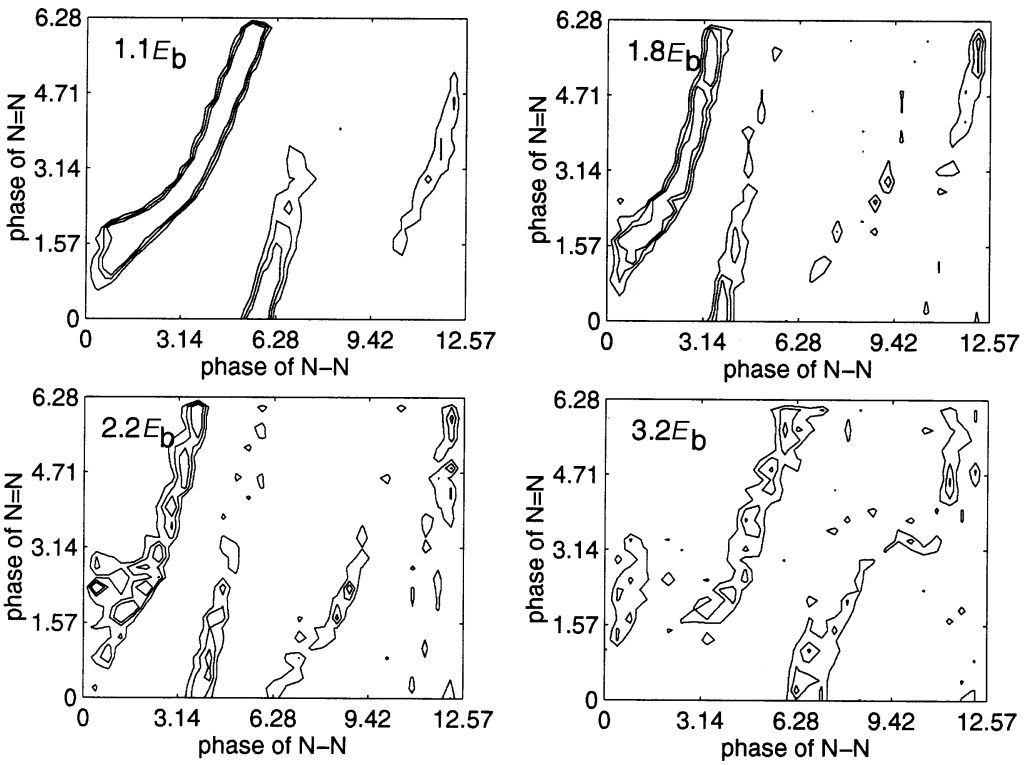

Fig. 16 Contoured phase maps of the N=N stretch local modes for 100 HN_3 trajectories with energies varying between $1.1E_b$ and $3.2E_b$. Phases are in radians.

total energy is only slightly in excess of that required for reaction ($1.1E_b$) phase pairings between the N=N stretch and the reaction coordinate are strongly constrained for the entire final vibration, in such a manner that during the final cycle the two stretching modes contract nearly in unison. Near the inner turning point ($\phi = \pi$) a change occurs such that the reaction coordinate extends more rapidly than does the N=N stretch, with reaction as the culmination of this final extension. The sharpness of the contoured region in this plot shows that substantially all of the one hundred trajectories calculated followed this pattern of motions. As we examine the contoured phase maps for higher energies we see that while this series of motions remains the favored path to reaction, as energy increases other paths also become viable. This is apparent as a loss of organization in the phase maps, as a wider range of phase pairings between these two vibrations still permit reaction.

6 Conclusions and discussion

The ability to identify patterns in the motions of atoms during reaction affords us insight into the process of chemical reaction. Traditionally, reaction dynamics have been studied in time, but (because of anharmonicity) patterns of motions that are evident in phase may be obscured in time. Comparison of reactions in phase (*i.e.*, coherently) requires a mechanism for transforming from time to phase, and to this end we introduce a new application of the Hilbert transform, which can assign consistent phase values to the vibrations of coupled anharmonic oscillators, irrespective of the energy and degree of anharmonicity. The Hilbert transform phase therefore is appropriate for coherent comparison of trajectories.

When we study the reaction dynamics of HN_3 in terms of phase we find that patterns of motion become more evident. In particular, it becomes apparent that the motions of several local modes (especially the terminal N=N stretch) correlate with those of the reaction coordinate during the final stages of reaction. This result is interesting because prior to the final few vibrations the motions of these local modes are uncorrelated, and no pattern can be discerned when one compares a large number of reactions. However, commencing roughly two vibrations prior to reaction the relative motions of these vibrations cease to be random, and all reactive trajectories converge on a narrow range of phase relationships. The formerly unrelated vibrations combine (for a short period preceding reaction) to form a single mode, and the result of this combination is reaction. We refer to this synchronization of motions between local modes and the reaction coordinate during reaction as correlated motion. While this paper focuses on correlated motion in the reaction dynamics of HN_3, conditions giving rise to correlated motion are not specific to this molecule.

We have proposed a model for correlated motion as a consequence of the requirements for energy to transfer from orthogonal modes into the reaction coordinate. If (as is the case with HN_3) one or more local modes couple strongly to the reaction coordinate then correlated motion will result. However, should the local mode be isolated from the reaction coordinate then no correlated motion is observed. That correlated motion is a consequence of energy transfer is directly observable from tornado plots. Recall that these plots are generated by plotting space curves corresponding to the phase space ellipse of an oscillator, and that the radius of the resulting helix is related to the oscillator energy. Close examinations of the right tornado plot in Fig. 14 shows two distinct helicies, with z ranging from 0 to 10 corresponding to a helix with a small radius, and z values from 20 to 40 corresponding to a much larger radius helix, and the intervening range of z from 10 to 20 corresponding to the transition between the two. Recall also that large z values correspond to reactant states of the molecule and $z = 0$ to the transition state. The tornado plot is interpreted in physical terms to show that until the stage of reaction marked by $z = 20$, the terminal N=N vibration is an energetic one with a large amplitude motion. During the stage of reaction delimited by $z = 20$ to $z = 10$, energy is transferred out of this mode. In advance of the energy transfer, trajectories converge in phase, changing from a featureless swirl, wherein phases are random, into a well-defined bundle, characterized by a restricted set of phase values. The importance of phase to energy transfer is evident because the trajectories must converge in phase before energy transfer begins. When trajectory phases are strongly converged ($z \approx 20$) the N=N vibration next gives up its excess energy to the reaction coordinate, resulting in a lower amplitude vibration lasting from $z = 10$ to $z = 0$, when reaction occurs. Independent calculations[2] verify that energy indeed transfers from the N=N stretch into the reaction coordinate during reaction.

But what do we mean by the reaction coordinate? Although we have been using this term to refer only to the bond that ultimately breaks, the existence of correlated motion suggests that the reaction coordinate is not simply the breaking bond, but is an admixture of that bond and of all other local modes whose motions correlate with those of the breaking bond. It is the synchronization of those motions which allows energy transfer (resulting in reaction) so from this perspective reaction is a consequence of all the contributing motions. We therefore choose to characterize the reaction coordinate as a linear combination of all modes with correlated motion. However, Fig. 15 shows that the contribution of a local mode to the reaction coordinate can change with energy. This result is unsurprising, as (because of anharmonicity) molecular modes of motion continually evolve with increasing total energy.

Fig. 14 shows that coupling between a local mode and the breaking bond is necessary for correlated motion, but does not address the issue of why this should be. Towards this end we have reduced the HN_3 system to its bare essentials, a two-dimensional model whose Hamiltonian is as follows:

$$H(s_1, s_2, p_1, p_2) = V_1(s_1) + V_2(s_2) + \tfrac{1}{2}\boldsymbol{P}^{\dagger}\boldsymbol{G}\boldsymbol{P} \qquad (8)$$

where V_1 and V_2 are Morse oscillators corresponding to the N=N dissociative mode and the N=N nondissociative one, $\boldsymbol{P}$ is the column vector (p_1, p_2) and $\boldsymbol{P}^{\dagger}$ is its transpose. The two stretching modes are coupled kinetically through an off-diagonal term in the Wilson $\boldsymbol{G}$ matrix.[24] In Fig. 17 we show the final vibration for fifty reactive trajectories, superimposed upon the potential energy surface (PES) for this model. In this

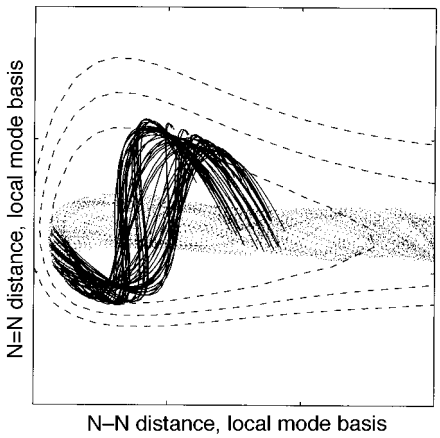

Fig. 17 The final oscillation for fifty reactive trajectories is superimposed upon the PES, which is that of two Morse oscillators. Both the trajectory paths and the energy contours are expressed in local mode coordinates. For clarity, the trajectories are plotted using a solid line for the first half cycle of vibration and a dotted one for the second half cycle, culminating at the right hand side in reaction.

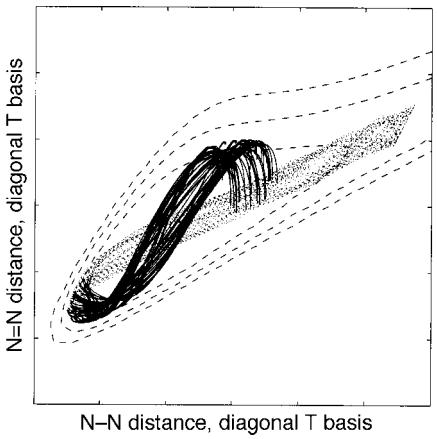

Fig. 18 The final oscillation for fifty reactive trajectories is superimposed upon the PES, which is that of two Morse oscillators. Both the trajectory paths and the energy contours are expressed in coordinates in which the kinetic energy term is diagonal. For clarity the trajectories are plotted using a solid line for the first half cycle of vibration and a dotted one for the second half cycle, culminating at the right hand side in reaction.

figure the nominal reaction coordinate (*i.e.*, the breaking bond) is the *x*-axis, and the *y*-axis is the N=N bond distance. When we examine the path of these reactive trajectories, only in the final stages (*i.e.*, the range shown in dots) is it apparent that reaction is inevitable. At the beginning of the final vibration (*i.e.*, the range shown by the solid lines) it is not apparent that these trajectories are aligned and ready to react. This perspective, of viewing the reaction coordinate as only the breaking bond, is deceptive. We can incorporate the concept of correlated motion by forming a reaction coordinate which is a linear combination of both participating local modes, *i.e.*, the bond that ultimately breaks and the bond that donates the energy to cause the dissociation. Fig. 18 shows both the PES and the trajectories plotted in a rotated basis where the kinetic energy term of the Hamiltonian is now diagonal. In this rotated basis the kinetic coupling term between these two stretches (which was previously identified as being the term critical to their correlated motion) is now incorporated into the revised shape of the rotated PES. In this rotated frame it is now apparent that all trajectories are poised to react, aligned with the reaction coordinate, which is clearly a linear combination of both the N—N and the N=N stretches.

We therefore propose that for molecules with correlated motion the reaction coordinate should be considered to be a linear combination of all modes exhibiting correlated motion, with a contribution to the reaction coordinate proportional to the strength of the correlation of the local mode. We further conclude that correlated motion is a consequence of constraints to energy transfer, such that in molecules with correlated motion the flow of energy between modes is dependent upon the relative phases of their vibrations.

Acknowledgements

This work was conducted with partial support from the Robert A. Welch Foundation of Houston, Texas. One of us (K.R.W.) would also like to thank Dr. John Parrish and Dr. Bruce Johnson for helpful discussions regarding the Hilbert transform.

References

1 L. G. Spears, Jr. and J. S. Hutchinson. *J. Chem. Phys.*, 1988, **88**, 250.
2 V. Julien, A. Patel, Y. Jones, J. Jiang and J. S. Hutchinson, *J. Phys. Chem.*, 1993, **97**, 7011.
3 J. S. Hutchinson, *Adv. Classical Trajectory Methods*, 1992, **1**, 41.
4 J. R. Fair, K. R. Wright and J. S. Hutchinson, *J. Phys. Chem.*, 1995, **99**, 14707.
5. J. S. Hutchinson, in *Dynamics of Molecules and Chemical Reactions*, ed. R. E. Wyatt and J. Zhang, Marcel-Dekker, New York, 1996, ch. 14, p. 561.
6 N. De Leon and C. C. Marston, *J. Chem. Phys.*, 1989, **91**, 3405.
7 N. De Leon, M. A. Mehta and R. Q. Topper, *J. Chem. Phys.*, 1991, **94**, 8310.
8 N. De Leon, *J. Chem. Phys.*, 1992, **96**, 285.
9 N. De Leon and S. Ling, *J. Chem. Phys.*, 1994, **101**, 4790.
10 M. H. Alexander, H-J. Werner, T. Hemmer and P. J. Knowles *J. Chem. Phys.*, 1990, **93**, 3307.
11 B. R. Foy, M. P. Casassa, J. C. Stephenson and D. S. King, *J. Chem. Phys.*, 1988, **89**, 608.
12 E. J. Heller, *J. Chem. Phys.*, 1975, **62**, 1544.
13 H. Goldstein, *Classical Mechanics*, Addison-Wesley, Reading, MA, 2nd edn., 1980.
14 P. D. Spanos and S. M. Miller, *J. Appl. Mech. Trans. ASME*, 1994, **61**, 575.
15 K. E. Peiponen, E. M. Vartiainen and T. Asakura, *Optik*, 1992, **90**, 45.
16 N. L. Mohan, *Geophysics*, 1982, **47**, 376.
17 C. P. Williams and A. G. Marshall, *Anal. Chem.*, 1992, **64**, 916.
18 J. E. Bertie and S. L. L. Zhang, *Can. J. Chem.*, 1992, **70**, 520.
19 A. J. Marshall, *Fourier, Hadamard, and Hilbert Transforms in Chemistry*, Plenum Press, New York, 1982.
20 D. S. Hagen, J. H. Weiner and B. D. Sykes, *Biochemistry*, 1979, **18**, 2007.
21 C. P. Poole, Jr., *Electron Spin Resonance*, Interscience, New York, 1967.
22 R. N. Bracewell, *The Fourier Transform and its Applications*, McGraw Hill, New York, 1978.
23 G. Arfken, *Mathematical Methods for Physicists*, Academic Press, New York, 3rd edn., 1970.
24 E. B. Wilson, Jr., J. C. Decius and P. C. Cross, *Molecular Vibrations: The Theory of Infrared and Raman Vibrational Spectra*, Dover Publications, New York, 1955.

Paper 8/08134D